Unusual spectral renormalization in hexaborides

2011 J. Phys.: Condens. Matter 23 495601

(http://iopscience.iop.org/0953-8984/23/49/495601)

IOP PUBLISHING JOURNAL OF PHYSICS: CONDENSED MATTER
J. Phys.: Condens. Matter **23** (2011) 495601 (6pp) doi:10.1088/0953-8984/23/49/495601

Unusual spectral renormalization in hexaborides

Swapnil Patil[1], Ganesh Adhikary[1], G Balakrishnan[2] and Kalobaran Maiti[1]

[1] Department of Condensed Matter Physics and Materials Science, Tata Institute of Fundamental Research, Homi Bhabha Road, Colaba, Mumbai 400005, India
[2] Department of Physics, University of Warwick, Coventry CV4 7AL, UK

E-mail: kbmaiti@tifr.res.in

Received 5 August 2011, in final form 20 October 2011
Published 17 November 2011
Online at stacks.iop.org/JPhysCM/23/495601

Abstract
Employing high resolution photoemission spectroscopy, we studied the evolution of the spectral features in rare earth hexaboride single crystals as a function of temperature and 4f binding energy, where the variation of the 4f binding energy is obtained by changing the rare earth element. High energy resolution helped to reveal the distinct features corresponding to the various photoemission final states. Experimental results of CeB_6, a dense Kondo system, exhibit the growth of the features near the Fermi level with the decrease in temperature relative to the uncompensated local moment contributions. The valence band spectra of the antiferromagnetic compounds, PrB_6 and NdB_6, exhibit multiple features—the 4f ionization peaks (poorly screened features) appear at higher binding energies and the features in the vicinity of the Fermi level possessing significant 4f character are due to the well-screened photoemission final states. These results indicate finite hybridization between the 4f and B 2s2p conduction electronic states. Interestingly, the well-screened features in PrB_6 and NdB_6 exhibit unusual enhancement in intensity at low temperature.

(Some figures may appear in colour only in the online journal)

1. Introduction

Hexaborides with the general formula unit RB_6 (R = rare earths) are an interesting class of compounds and attracted a lot of attention due to the finding of varied interesting properties in these systems [1]. They form in a cubic crystalline structure, where B_6 octahedra occupy the cube corners, creating a large void space at the body center for the rare earth sites to occupy. Thus, hexaborides are structurally quite independent of the size of the rare earth atoms [2]. B 2s2p electrons form the valence band in these materials, which is very similar across the series for rare earth substitutions [3]. Depending on the occupancy of the 4f band and binding energy, ϵ_{4f} of 4f electrons, hexaborides exhibit a plethora of interesting properties. For example, LaB_6 is a good metal [4], CeB_6 is a dense Kondo system [5], PrB_6 and NdB_6 are antiferromagnetic metals ($T_N \sim 7$ K) [6, 7], SmB_6 is a Kondo insulator [8], EuB_6 is a ferromagnetic semiconductor [9], etc.

In this paper, we studied the evolution of the electronic structure of RB_6 (R = La, Ce, Pr and Nd) as a function of both temperature and the impurity band binding energy, ϵ_{4f}, employing state-of-the-art energy-resolved photoemission spectroscopy. ϵ_{4f} increases as one goes from La towards the right in the rare earth series. The photoemission spectra in this study exhibit the distinct signature of finite hybridization of the 4f electrons with the conduction electrons in all the compounds studied. The well-screened features appearing near the Fermi level exhibit large 4f character and interesting temperature evolution.

2. Experimental details

The samples were grown in single-crystalline form by the floating zone technique using a four-mirror Xe arc lamp image furnace. The growths were carried out in a flow of argon gas and growth speeds of 10–18 mm h^{-1} [10]. The photoemission measurements were performed using a Gammadata Scienta SES2002 analyzer and monochromatic photon sources with energy resolution of 300 meV at $h\nu = 1486.6$ eV (Al Kα) and 2 meV at $h\nu = 21.2$ eV (He I) and 40.8 eV (He II) photon

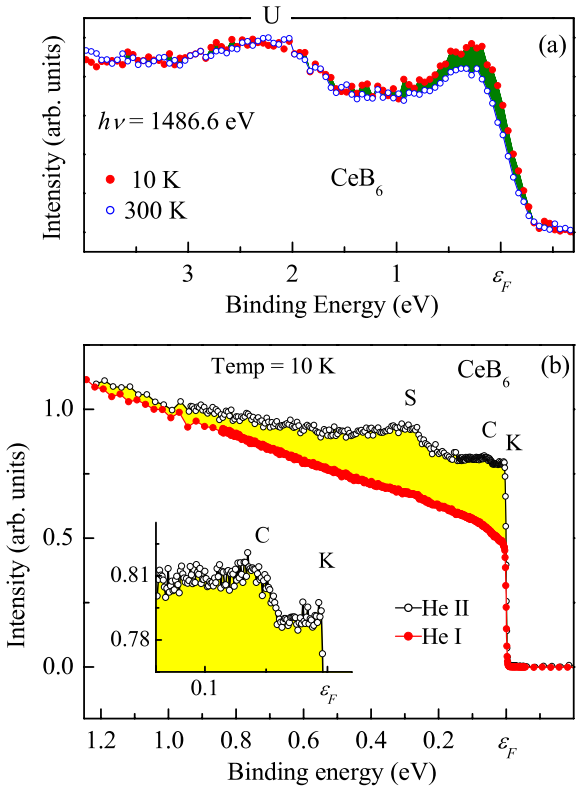

Figure 1. (a) Al Kα spectra of CeB_6 at 10 and 300 K showing interesting temperature evolution. (b) High resolution He II spectrum (open circles) and He I spectrum (solid circles) of CeB_6 at 10 K. The inset shows the expanded view of the He II spectrum at 10 K.

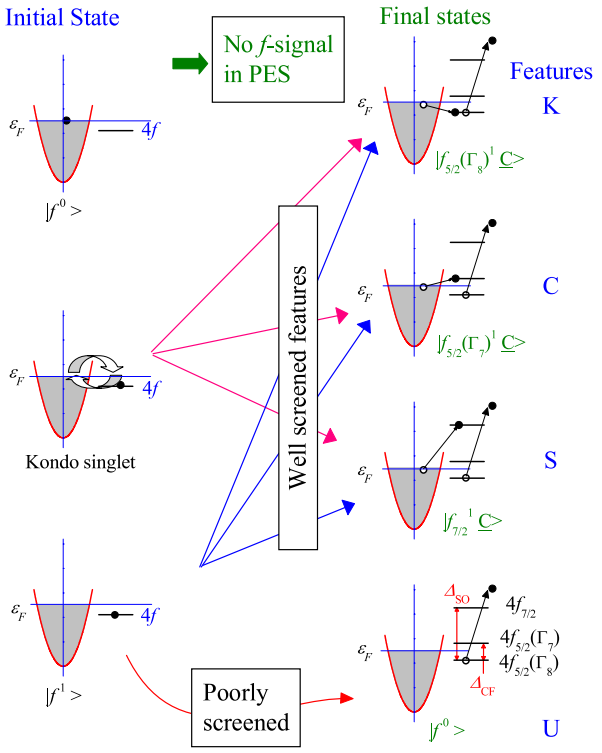

Figure 2. Schematic representation of the Ce 4f photoemission leading to different final states.

energies. The samples were cleaved at a base pressure better than 3×10^{-11} Torr to expose the clean sample surface for photoemission measurements. The cleanliness of the surface was confirmed by the absence of the impurity features in the x-ray photoemission (XP) spectra. It was observed that small impurity features appeared in the XP spectra about 6–7 h after the cleaving and hence several cleaning cycles were necessary although the base pressure of the spectrometer chamber was maintained at better than 3×10^{-11} Torr. We also verified that the angle-integrated data collected on a cleaved surface and scraped surface using a fine grain diamond file were identical. Reproducibility of the spectra were confirmed after each cleaving/scraping. The temperature variation down to liquid helium temperature was achieved using an open cycle (pumped) He cryostat LT-3M from Advanced Research Systems, USA.

3. Results and discussions

The valence band spectra of CeB_6 obtained by x-ray photoemission (XP) spectroscopy ($h\nu = 1486.6$ eV) at 10 and 300 K are shown in figure 1(a). There are two distinct and intense photoemission [13] features visible in both spectra; one at 2.1 eV denoted by U and the other near the Fermi level, ϵ_F. At this photon energy, the probing depth of photoemission spectroscopy is quite a bit larger than what is obtained at lower photon energies, for example in the vacuum ultraviolet regime [11]. Therefore, these features can be attributed to the bulk electronic structure of this system [14]. Moreover, the significantly large photoemission cross section of the Ce 4f states relative to that for the B 2s2p states at Al Kα photon energies suggests that these features possess dominant Ce 4f character [20]. A normalization by the intensity of U reveals that the 10 K spectrum possesses significantly larger intensity at ϵ_F compared to that in the 300 K spectrum.

In order to investigate the near ϵ_F feature further, we have performed experiments in this binding energy range with high energy resolution of about 2 meV using ultraviolet (UV) photon energies. The spectra are shown in figure 1(b). The near ϵ_F intensities exhibit three distinct features denoted by S, C and K in the high resolution He II spectra at 10 K as shown by open circles in figure 1(b). The He I spectrum collected at the same temperature and setting shown by solid circles in the figure do not exhibit these features establishing again their dominant 4f character. All these features exhibit an enhancement in intensity as the temperature is lowered.

It is realized that the periodic Anderson model is necessary to derive the microscopic details of such systems. However, photoemission is a local phenomena and therefore the single impurity Anderson model has often been found to capture well the essential features such as the final state character of the photoemission features. Thus, the character of the photoemission spectral features in CeB_6 can be learnt following the Gunnarsson–Schönhammer picture [15] based on the impurity Anderson model as shown schematically in figure 2.

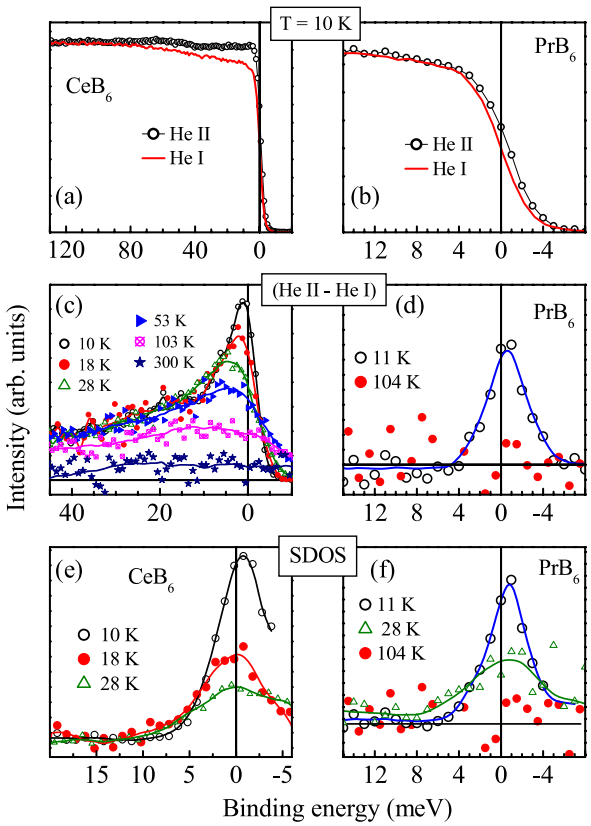

Figure 3. (a) and (b) shows the high resolution He I and He II spectra at 10 K of CeB_6 and PrB_6. (He II–He I) spectra at different temperatures for (c) CeB_6 and (d) PrB_6 exhibiting temperature evolution of the Kondo peak. The spectral density of states of (e) CeB_6 and (f) PrB_6 obtained by dividing the He II spectra by the resolution-broadened Fermi–Dirac distribution function.

In CeB_6, there is one electron in the 4f level. Due to the proximity of the 4f energy level to the Fermi level, this electron will hop back and forth between the conduction band and the 4f level. Therefore, the initial state of photoexcitation will be a linear combination of $4|f^0\rangle$ (an f electron has hopped to the conduction band) and $4|f^1\rangle$ electronic configurations. In the event of the conduction electrons strongly coupled to the 4f moment antiparallely, there will an additional contribution from a Kondo singlet state, $(4|f_{\Uparrow}\rangle|c_{\downarrow}\rangle - 4|f_{\Downarrow}\rangle|c_{\uparrow}\rangle)$ at low temperatures. Therefore, the initial state can be expressed as

$$|i\rangle = 4|f^0\rangle + 4|f^1\rangle + (4|f_{\Uparrow}\rangle|c_{\downarrow}\rangle - 4|f_{\Downarrow}\rangle|c_{\uparrow}\rangle).$$

The photoexcitation of an 4f electron creates a hole in the 4f band. If the 4f hole remains unscreened in the final state ($4|f^n\rangle \Rightarrow 4|f^{n-1}\rangle$ transition), the feature is called a poorly screened feature or ionization peak. The feature, U in figures 1 and 2, can be attributed to such a photoemission process. The binding energy of this feature provides an estimation of ϵ_{4f}.

The other possible final states correspond to the $4|f^n\rangle \Rightarrow 4|f^n\underline{c}\rangle$ transition, where a conduction electron hops to the 4f level at the photoemission site to screen the photo-hole, creating a hole, $\underline{c}$ in the conduction band. The spin–orbit coupling and crystal field effect will lift the degeneracy of the f band [16]. Since the photoemission final state is an excited state, the angular momentum, $j(=l \pm s)$ of the final state 4f electron will be 7/2 and 5/2 due to the spin–orbit splitting. Due to the cubic crystal field, $|f_{5/2}\rangle$ splits further to $|f_{5/2}(\Gamma_8)\rangle$ and $|f_{5/2}(\Gamma_7)\rangle$. The corresponding splitting of $|f_{7/2}\rangle$ state will not be visible in the experimental spectra due to the large photo-hole lifetime broadening at higher binding energies. Thus, the features S, C and K can be assigned to the final state configurations $|f^1_{7/2}\underline{c}\rangle$, $|f_{5/2}\,(\Gamma_7)^1\,\underline{c}\rangle$ and $|f_{5/2}\,(\Gamma_8)^1\,\underline{c}\rangle$, respectively. The energy separation of the features S–K provide an estimate of the spin–orbit coupling strength, $\Delta_{SO} \approx 280$ meV. The energy difference between the features C and K provides an estimate of the crystal field splitting, Δ_{CF}, which is found to be about 50 meV.

It is to be noted here that the three features corresponding to the well-screened final states in the photoemission spectra may appear from the initial states $4|f^1\rangle$ as well as from $(4|f_{\uparrow}\rangle|c_{\downarrow}\rangle - 4|f_{\downarrow}\rangle|c_{\uparrow}\rangle)$. However, the contribution to U from the Kondo singlet initial state photoemission is negligible as the conduction electrons are entangled with the 4f states and hence will screen the f hole immediately a photo-hole is created. Therefore, the intensity of C, S and K with respect to U will grow as the temperatures is lowered due to the contribution from Kondo singlet initial states, as such states appear only at low temperatures. Moreover, 4f electrons corresponding to $|4f^1\underline{c}\rangle$ final states may also be entangled with the conduction electrons leading to an additional temperature dependence of the features C, S and K. Thus, the temperature dependence of the relative intensities of the features possessing 4f character manifests characteristics of the Kondo effect—the intensity enhancement of C, S and K relative to U in figure 1 with reducing temperature could, therefore, be a case of the Kondo effect [17][3]. Note that the Kondo resonance feature appearing at the Fermi level in the initial state can have different binding energies in the photoemission spectral function as the binding energy scale of the photoemission spectra is derived from the final state Hamiltonian of the photoemission process.

We exploit the incident photon energy dependence of the photoemission cross section Ω to delineate the 4f-related features in the experimental spectra. Ω(B 2p) = 1.934 and 0.4227; Ω(La 5d) = 4.085 and 0.5192; Ω(Ce 4f) = 0.6255 and 2.033 at He I and He II energies, respectively [20]. Evidently, the change in photon energy from He I to He II leads to a significant enhancement in the 4f cross section while it decreases in all other cases. Thus, the difference, (He II–He I), provides a good estimation of the 4f contributions. In figures 3(a) and (b), we show the high resolution He I (line) and He II spectra (symbols) collected at 10 K of CeB_6 and PrB_6, respectively[4]. The intensity at the Fermi level is higher in the He II spectra than the

[3] The lattice volume does not change at the temperatures investigated [2, 19]. Therefore, the hybridization and the on-site Ce 4f Coulomb correlation strength [18] are not expected to change with temperature.

[4] Here, the spectra are normalized by the intensity between the crystal field peak and spin–orbit peak (∼150 meV binding energy) after collecting the spectra in this energy range with good signal-to-noise ratio. This normalization is different from the one used in figure 1(b) and rescales the peak intensity, keeping the temperature dependence of the peaks almost unchanged.

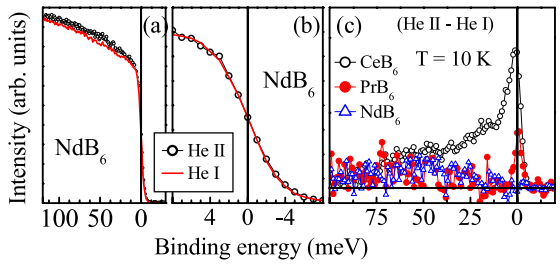

Figure 4. High resolution He I and He II spectra of NdB_6 at 10 K are shown in (a) and the same in an expanded energy scale in (b). (c) (He II–He I) spectra of CeB_6, PrB_6 and NdB_6 exhibiting a signature of finite intensity around 50 meV in all cases.

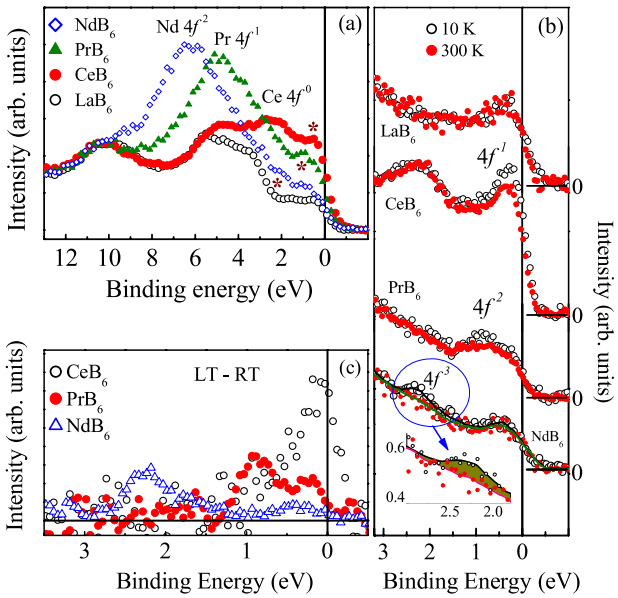

Figure 5. (a) Al Kα spectra of LaB_6, CeB_6, PrB_6 and NdB_6 at 10 K. (b) Comparison of the high resolution Al Kα spectra at 10 K (LT) and 300 K (RT). (c) The difference spectra (RT–LT). The signature of Kondo resonance feature even in PrB_6 and NdB_6 is revealed although no Kondo effect is observed in their bulk physical properties.

intensity in the He I spectra in both cases. To bring out clarity in the difference between the two spectra, we plot the difference spectra, (He II–He I) in figures 3(c) and (d) for CeB_6 and PrB_6, respectively. The 4f contribution at ϵ_F is quite strong in CeB_6 and becomes significantly smaller in the heavier rare earth hexaboride, PrB_6, presumably due to the reduction in hybridization strength V_{cf} between the 4f states and conduction electronic states with the increase in ϵ_{4f} in these systems.

The temperature dependence of the difference spectra for CeB_6 is shown in figure 3(c). The sharp features seen at 10 K gradually reduce in intensity with the increase in temperature. Finite temperature leads to a significant redistribution of the spectral density of states around the Fermi level as depicted by the Fermi–Dirac distribution function. Therefore, we derived the spectral density of states (SDOS) by dividing the He II spectra by the resolution-broadened Fermi–Dirac distribution function—the results are shown in figure 3(e). The features in figures 3(c) and (e) obtained following different procedures are quite similar, suggesting that the presence of the feature is independent of the data analysis and possesses a direct correspondence to the raw data shown in figure 3(a). The same exercise in PrB_6 spectra (see figures 3(d) and (f)) reveals sharp features at ϵ_F possessing 4f character at 10 K, which vanishes at 104 K indicating strong temperature dependence.

The He I and He II spectra of NdB_6 collected at 10 K are shown in figure 4(a) and in an expanded energy scale in figure 4(b). It appears that the intensity around 50 meV binding energy is somewhat stronger in the He II spectrum compared to the intensity of the He I spectrum. The intensity at the Fermi level is found to be identical. In order to visualize the change in intensity better, we plot the (He II–He I) spectra at 10 K of all the three compounds CeB_6, PrB_6 and NdB_6 in figure 4(c). The intensity around 50 meV in the difference spectra appears to be finite in all the cases. However, the features becomes more and more weaker at the Fermi level as one goes towards heavier rare earths.

The relative photoemission cross section of 4f states at Al Kα photon energy is about three orders of magnitude higher than that of the other (B 2s2p) valence states [20]. Therefore, XP spectra are a good representation of the 4f contributions. We investigate the XP valence band spectra of RB_6; R = La, Ce, Pr and Nd. The spectra taken at T = 10 K are shown in figure 5(a). The LaB_6 valence band is essentially formed by B 2s 2p states [21]. Since non-f density of states are similar in this class of compounds [3], all the spectra are normalized by the intensity of the feature around 10 eV essentially contributed by B 2s2p states. In every case, distinct signatures of ionization and screened peaks are visible. The ionization peaks in CeB_6, PrB_6 and NdB_6corresponding to the final states possessing $4f^0$, $4f^1$ and $4f^2$ electronic configurations appear at about 2.1 eV, 5 eV and 6.25 eV binding energies, respectively. The screened peaks possess $4f^1$ (for CeB_6), $4f^2$ (for PrB_6) and $4f^3$ (for NdB_6) electronic configurations and appear nearer to ϵ_F marked by '$\star$' in figure 5(a) [22, 23].

The temperature dependence of the intensities near ϵ_F is shown in figure 5(b) after normalizing them by the intensity of the ionization peak. The spectra for LaB_6 do not show an observable change with temperature. This suggests that B 2s2p electronic states are not sensitive to temperature. This also confirms that the phonon-induced effects [24] will be weak in this class of system as it is expected to be similar in all cases. The spectra for CeB_6 exhibit strong enhancement of the well-screened feature presumably due to Kondo-type interactions as discussed earlier. Interestingly, we observe an enhancement of the spectral weight in the case of PrB_6 and NdB_6 too at 10 K relative to the 300 K spectra as also shown in figures 3 and 4. The enhancement of the 4f spectral intensity can clearly be visible in the difference spectra[5] shown in figure 5(c) exhibiting distinct features grown at 10 K for

[5] Difference spectra = 10 K spectra − 300 K spectra. In NdB_6, the subtraction is done between the smooth curves drawn through the experimental points.

all the samples with one peak near ϵ_F and the other one systematically moving towards higher binding energies as ϵ_{4f} enhances.

Following the schematic representation due to the final state effects, the higher binding energy peak can be attributed to the spin–orbit splitting, which appears at 0.9 eV for PrB_6 and 2.3 eV for NdB_6 [25]. The bulk properties of PrB_6 and NdB_6 were studied extensively in the past [7, 12]. Although one cannot rule out the possibility of the presence of resistivity minima as a flattening in resistivity occurs around 25 K in both cases [12], a distinct signature of Kondo behavior in their transport and magnetic properties is not evident. Thus, such photoemission spectral renormalization is puzzling.

On the other hand, it is well known that sharp features near ϵ_F can appear from bare band structure results, photoemission cross section effects and/or photoemission final state effects. Insensitivity of the LaB_6 spectra to temperature rules out a strong phonon broadening effect. Another possibility could be the formation of spin-polaron polarization of the 5d electrons and/or conduction electrons due to the 4f moment, which exhibits a similar temperature dependence [26]. In such a case, the features will possess 5d and/or B 2s2p character in contrast to the finding of the 4f character here. Although the spectral evolution in PrB_6 and NdB_6 seems puzzling, it is evident that both Pr 4f and Nd 4f levels are hybridized with the conduction electronic states leading to the appearance of the well-screened features—consistent with the earlier studies [27]. Further studies of the spectral function along with transport analysis [28] are necessary to understand these unusual phenomena.

4. Conclusions

Employing high resolution photoemission spectroscopy, we studied the spectral evolution of a series of hexaborides RB_6 exhibiting varied interesting bulk properties. The finite hybridization between 4f electronic states and the conduction electrons is manifested by the finite intensity of the well-screened features in the photoemission spectra. A decrease in temperature leads to an enhancement of the well-screened feature intensity relative to the unscreened feature intensity indicating the signature of a generic phenomenon in correlated electron systems [29].

Acknowledgments

SP thanks the Council of Scientific and Industrial Research, Government of India for financial support. GB thanks EPSRC, UK, for financial support for the crystal growth activities.

References

[1] Ji X H, Zhang Q Y, Xu J Q and Zhao Y M 2011 *Prog. Solid State Chem.* **39** 51
[2] Takahashi Y, Ohshima K-I, Okamura F P, Otani S and Tanaka T 1999 *J. Phys. Soc. Japan* **68** 2304
[3] Kimura S, Nanba T, Tomikawa M, Kunii S and Kasuya T 1992 *Phys. Rev.* B **46** 12196
[4] Nishitani R, Aono M, Tanaka T, Oshima C, Kawai S, Iwasaki H and Nakamura S 1980 *Surf. Sci.* **93** 535
[5] Samwer K and Winzer K 1976 *Z. Phys.* B **25** 269
[6] Geballe T H, Matthias B T, Andres K, Maita J P, Cooper A S and Corenzwit E 1968 *Science* **160** 1443
[7] Sera M, Kobayashi S, Hiroi M, Kobayashi N and Kunii S 1996 *Phys. Rev.* B **54** R5207
Ali N and Woods S B 1982 *J. Appl. Phys.* **53** 7905
[8] Nyhus P, Cooper S L, Fisk Z and Sarrao J 1997 *Phys. Rev.* B **55** 12488
[9] Guy C N, von Molnar S, Etourneau J and Fisk Z 1980 *Solid State Commun.* **33** 1055
[10] Balakrishnan G, Lees M R and Paul D 2003 *J. Cryst. Growth* **256** 206
Balakrishnan G, Lees M R and Paul D 2004 *J. Magn. Magn. Mater.* **272–276** 601
[11] Maiti K, Manju U, Ray S, Mahadevan P, Inoue I H, Carbone C and Sarma D D 2006 *Phys. Rev.* B **73** 052508
Maiti K, Kumar A, Sarma D D, Weschke E and Kaindl G 2004 *Phys. Rev.* B **70** 195112
Maiti K and Sarma D D 2000 *Phys. Rev.* B **61** 2525
Maiti K and Singh R S 2005 *Phys. Rev.* B **71** 161102(R)
Maiti K, Singh R S and Medicherla V R R 2007 *Phys. Rev.* B **76** 165128
[12] Onuki Y, Umezawa A, Kwok W K, Crabtree G W, Nishihara M, Yamazaki T, Omi T and Komatsubara T 1989 *Phys. Rev.* B **40** 11195
[13] Chiaia G *et al* 1997 *Phys. Rev.* B **55** 9207
[14] Patil S, Adhikary G, Balakrishnan G and Maiti K 2010 *Appl. Phys. Lett.* **96** 092106
Patil S, Adhikary G, Balakrishnan G and Maiti K 2011 *Solid State Commun.* **151** 326
Maiti K, Patil S, Adhikary G and Balakrishnan G 2011 *J. Phys.: Conf. Ser.* **273** 012042
[15] Gunnarsson O and Schönhammer K 1983 *Phys. Rev.* B **28** 4315
[16] Souma S, Kumigashira H, Ito T, Sato T, Takahashi T and Kunii S 2001 *J. Electron Spectrosc. Relat. Phenom.* **114–116** 729
Loewenhaupt M and Prager M 1986 *Z. Phys.* B **62** 195
[17] Patthey F, Schneider W-D, Baer Y and Delley B 1987 *Phys. Rev. Lett.* **58** 2810
Patthey F, Schneider W-D, Baer Y and Delley B 1990 *Phys. Rev.* B **42** 8864
Garnier M, Breuer K, Purdie D, Hengsberger M, Baer Y and Delley B 1997 *Phys. Rev. Lett.* **78** 4127
Ehm D, Hüfner S, Reinert F, Kroha J, Wölfle P, Stockert O, Geibel C and Löhneysen H V 2007 *Phys. Rev.* B **76** 045117
Klein M, Nuber A, Reinert F, Kroha J, Stockert O and Löhneysen H V 2008 *Phys. Rev. Lett.* **101** 266404
Patil S, Iyer Kartik K, Maiti K and Sampathkumaran E V 2008 *Phys. Rev.* B **77** 094443
Patil S, Iyer Kartik K, Maiti K and Sampathkumaran E V 2010 *J. Phys.: Condens. Matter* **22** 255602
Patil S, Iyer Kartik K, Maiti K and Sampathkumaran E V 2010 *Phys. Rev.* B **82** 104428
[18] Gunnarsson O and Schönhammer K Jr 1987 *Handbook on the Physics and Chemistry of Rare Earths* vol 10, ed K A Gschneidner, L Eyring and S Hüfner (Amsterdam: Elsevier) pp 103–63
[19] Suzuki H, Xue Y, Hosomichi A, Naher S and Hata F 2006 *J. Supercond. Nov. Magn.* **19** 89
[20] Yeh J J and Lindau I 1985 *At. Data Nucl. Data Tables* **32** 1
[21] Medicherla V R R, Patil S, Singh R S and Maiti K 2007 *Appl. Phys. Lett.* **90** 062507
[22] Kalkowski G, Sampathkumaran E V, Laubschat C, Domke M and Kaindl G 1985 *Solid State Commun.* **55** 977

[23] Parks R D, Raaen S, denBoer M L, Chang Y-S and Williams G P 1984 *Phys. Rev. Lett.* **52** 2176
[24] Joyce J J, Arko A J, Lawrence J, Canfield P C, Fisk Z, Bartlett R J and Thompson J D 1992 *Phys. Rev. Lett.* **68** 236
[25] Goldschmidt Z B Jr 1978 *Handbook on the Physics and Chemistry of the Rare Earths* vol 1, ed K A Gschneidner and L Eyring (Amsterdam: North-Holland) pp 1–171
[26] Sluchanko N E, Bogach A V, Glushkov V V, Demishev S V, Ivanov V Yu, Ignatov M I, Kuznetsov A V, Samarin N A, Semeno A V and Shitsevalova N Yu 2007 *J. Exp. Theor. Phys.* **104** 120
Anisimov M A, Bogach A V, Glushkov V V, Demishev S V, Samarin N A, Filipov V B, Shitsevalova N Yu, Kuznetsov A V and Sluchanko N E 2009 *J. Exp. Theor. Phys.* **109** 815
[27] Fujimori A, Miyahara T, Koide T, Shidara T, Kato H, Fukutani H and Sato S 1988 *Phys. Rev.* B **38** 7789
[28] Vidhyadhiraja N S and Logan D E 2005 *J. Phys.: Condens. Matter* **17** 2959
Logan D E and Vidhyadhiraja N S 2005 *J. Phys.: Condens. Matter* **17** 2935
[29] Valla T, Johnson P D, Yusof Z, Wells B, Li Q, Loureiro S M, Cava R J, Mikami M, Mori Y, Yoshimura M and Sasaki T 2002 *Nature* **417** 627